

Research Article

One Clock-Cycle Response 0.5 μm CMOS Dual-Mode $\Sigma\Delta$ DC-DC Bypass Boost Converter Stable over Wide $R_{\text{ESR}}\text{LC}$ Variations

Neeraj A. Keskar¹ and Gabriel A. Rincón-Mora²

¹DC-DC Controllers, Texas Instruments, Manchester, NH 03054, USA

²Georgia Tech Analog, Power, and Energy IC Research Laboratory, School of ECE, Georgia Institute of Technology, Atlanta, GA 30332, USA

Correspondence should be addressed to Neeraj A. Keskar, neerajkeskar@ti.com

Received 29 April 2009; Accepted 21 January 2010

Academic Editor: Vassilios G. Agelidis

Copyright © 2010 N. A. Keskar and G. A. Rincón-Mora. This is an open access article distributed under the Creative Commons Attribution License, which permits unrestricted use, distribution, and reproduction in any medium, provided the original work is properly cited.

Power supplies in portable applications must not only conform and adapt to their highly integrated on-chip and in-package environments but also, more intrinsically, respond quickly to fast load dumps to achieve and maintain high accuracy. The frequency-compensation network, however, limits speed and regulation performance because it must cater to all combinations of filter capacitor C_O , inductor L , and C_O 's equivalent series resistance R_{ESR} resulting from tolerance and modal design targets. As such, it must compensate the worst-case condition and therefore restrain the performance of all other possible scenarios, even if the likelihood of occurrence of the latter is considerably high and the former substantially low. Sigma-delta ($\Sigma\Delta$) control, which addresses this issue in buck converters by easing its compensation requirements and offering one-cycle transient response, has not been able to simultaneously achieve high bandwidth, high accuracy, and wide $R_{\text{ESR}}\text{LC}$ compliance in boost converters. This paper presents a dual-mode $\Sigma\Delta$ boost bypass converter, which by using a high-bandwidth bypass path only during transient load-dump events was experimentally 1.41 to 6 times faster than the state of the art in current-mode $\Sigma\Delta$ boost supplies, and this without any compromise in $R_{\text{ESR}}\text{LC}$ compliance range (0–50 m Ω , 1–30 μH , and 1–350 μF).

1. Introduction

In portable applications like cellular phones, PDAs, and the like, integrated BiCMOS and CMOS switching dc-dc supply circuits reduce cost, size, component count, and design complexity (from a user's perspective). One of the critical bottlenecks in obtaining a fully integrated solution, however, is the frequency-compensation circuit, which is designed around off-chip power LC filter devices to obtain optimal performance [1]. The fact is mode-rich state-of-the-art applications, manufacturing tolerances, and parameter drifts expose dc-dc converter integrated circuits (ICs) to wide variations in output capacitance C_O , power inductance L , and C_O 's equivalent series resistance R_{ESR} , inducing considerable changes in loop-gain and transient response, compromising feedback stability or transient response. As a result, to guarantee stability and high bandwidth with a fixed on-chip frequency-compensation circuit, the design

necessarily constrains $R_{\text{ESR}}\text{LC}$ values within a narrow target range [1]. This is especially detrimental in compact high-performance multiple input-output converters [2, 3], where the on-chip or in-package LC filter is variable by design to dynamically accommodate the diverse loading conditions of the system.

Unlocked or asynchronous sigma-delta ($\Sigma\Delta$) buck converters [4–8] are self-compensating and free of the speed-stability tradeoffs of most dc-dc converters because the control loop in these converters resembles current-mode control by indirectly sensing the inductor current ripple via the ripple voltage it drops across C_O 's R_{ESR} . In other words, the ESR voltage mostly sets the terminal ripple voltage of C_O , impressing the inductor ripple current information on the output voltage and achieving current-mode-like control. The resulting single-pole-like response yields higher bandwidth and more explicit control over the output ripple voltage [7].

Extending this technique and its benefit to boost converters, which are popular in portable electronics for boosting battery voltages to 3.3–5 V, is not straightforward because the inductor current does not fully flow to C_O . Consequently, in realizing $\Sigma\Delta$ control in boost converters, the feedback circuit must explicitly sense and mix inductor current with the sensed output voltage [9]. Such techniques, however, resurrect the limiting speed-stability tradeoffs $\Sigma\Delta$ control averted in buck converters in the first place, forcing the designer to adjust current and voltage gains thereby reducing the loop bandwidth in order to accommodate large $R_{\text{ESR}}LC$ filter values.

This paper presents a dual-mode boost $\Sigma\Delta$ bypass controller IC that overcomes the aforementioned speed-stability compromise by introducing a high-speed bypass mode (and circuit) that engages only during transient load-dump events, achieving both high bandwidth and wide $R_{\text{ESR}}LC$ compliance. To this end, Section 2 first reviews and discusses the stability requirements of $\Sigma\Delta$ converters and their resulting transient response to fast load dumps. Section 3 then describes the proposed dual-mode technique and the design of its IC-prototype embodiment, followed by experimental results in Section 4; Section 5 draws relevant conclusions.

2. $\Sigma\Delta$ Converters

2.1. $\Sigma\Delta$ Control in Buck Converters. A $\Sigma\Delta$ buck converter, as shown in Figure 1, controls the frequency and duty cycle of PMOS switch S_M by comparing rippling output voltage v_O via sensed voltage v_S against dc reference V_{REF} with comparator CP_V . Operationally, ac inductor ripple current i_L flows into C_O and its R_{ESR} (which is relatively large in these converters at 100–250 m Ω to ensure its voltage $-v_{\text{esr}}$ overwhelms ac capacitor voltage v_c) [7] as capacitor displacement current i_c , forcing ac output ripple voltage v_o to mimic i_L ($v_o \approx v_{\text{esr}} = i_L R_{\text{ESR}}$). As a result, in regulating v_o , the converter also regulates i_L , which in the process simplifies the frequency response of the converter to that of a single-pole system, as in current-mode control, guaranteeing stability, irrespective of $R_{\text{ESR}}LC$ values.

In a positive load-step transient event, when load current i_O suddenly rises, comparator CP_V detects the voltage droop the now larger i_O induces on v_O and consequently switches S_M on indefinitely (i.e., at 100% duty cycle) until v_O returns within CP_V 's predefined hysteretic window limits, that is, within an acceptably low margin of V_{REF} . During S_M 's on time, the inductor voltage being nearly constant at $V_{\text{IN}} - V_O$, inductor current i_L slews in a single switching cycle until it fully supplies i_O and recharges C_O back to V_{REF} [8]. In other words, only the inductor and capacitor slew-rate limits and second-order delays across the comparator and switch set the response time (effective bandwidth) of the system. Note a negative load dump undergoes a similar but reversed response.

2.2. $\Sigma\Delta$ Control in Boost Converters. Unlike buck converters, ac inductor ripple current i_L in boost converters does not

flow completely to output capacitor C_O because reverse-biased diode D (shown in Figure 2) temporarily disconnects L from v_O (and C_O) when switch S_M conducts all of i_L to ground. The resulting ac ripple voltage in v_O does not fully reflect the behavior of i_L , as it does in buck converters with nonnegligible R_{ESR} values, which means that $\Sigma\Delta$ control in boost converters cannot rely on v_O alone [9]. The negative feedback loop in a boosting supply must therefore sense, scale, and mix i_L with v_O explicitly (e.g., mix $i_L R_I g_{mi}$ and $v_O g_{mv}$ into R_S as scaled sum v_{SUM}) to achieve current-mode-like control characteristics. A hysteretic comparator then modulates S_M 's frequency and duty cycle based on how the scaled sum (v_{SUM}) of the ripples compares against a user-defined hysteretic window. Note the voltage feedback loop modulates the effective inductor reference current $v_{I,\text{REF}}/R_I$, which is also the average inductor current I_L (or low-pass filtered—LPF—version of i_L) to whatever is necessary to fully supply i_O .

Within the context of averaged small-signal analysis, the relatively high-gain, low-bandwidth voltage control loop (V Loop) of the system effectively embeds a higher bandwidth, lower gain current loop (I Loop), as shown Figure 3 [10]. At low frequencies, below low-pass filter pole p_{LPF} , $i_L R_I$ nearly equals $v_{I,\text{REF}}$ and the gain of the current loop is practically zero, but increasing with frequency until reaching its highest possible gain at frequencies past p_{LPF} . The current loop's gain again drops at high frequencies, past the complex LC double poles, when the ac voltage across L decreases. Given that i_L is, for all practical purposes, regulated to higher frequencies and therefore is a current source to the outer voltage loop at moderate-to-high frequencies, C_O and effective load resistance R_O set the dominant low-frequency pole of the system while L and R_O invoke right-half plane zero z_{RHP} [11].

For stable conditions to prevail, the unity-gain frequency of the voltage loop (i.e., the system $-f_{V,0\text{dB}}$) must fall below z_{RHP} and i_L must remain a current source (i.e., current loop must stay closed with considerable loop gain) for the frequency range of interest to the voltage loop [10]. As such, $f_{V,0\text{dB}}$ must stay below both z_{RHP} and current-loop bandwidth $f_{I,0\text{dB}}$:

$$f_{0\text{dBV}} \approx \frac{g_{mv} D'_M}{2\pi R_I g_{mi} C_O} \ll f_{0\text{dBI}} \approx \frac{R_I g_{mi} R_S M V_O}{2\pi L}, \quad (1)$$

$$f_{0\text{dBV}} \approx \frac{g_{mv} D'_M}{2\pi R_I g_{mi} C_O} < z_{\text{RHP}} = \frac{D'_M V_O}{2\pi L I_L}, \quad (2)$$

or

$$\frac{L I_L}{V_O C_O} = \frac{L I_O}{C_O V_O D'_M} < \frac{R_I g_{mi}}{g_{mv}}, \quad (3)$$

where D_M is the duty-cycle of S_M , D'_M is $(1 - D_M)$, and M is the modulator gain. Note that z_{RHP} and $f_{I,0\text{dB}}$ shift to lower frequencies with increasing inductance values, which means that $f_{V,0\text{dB}}$ must also decrease accordingly, in an ideal case. LPF pole p_{LPF} , whose location indicates the lowest frequency at which the current loop is closed, must also be below

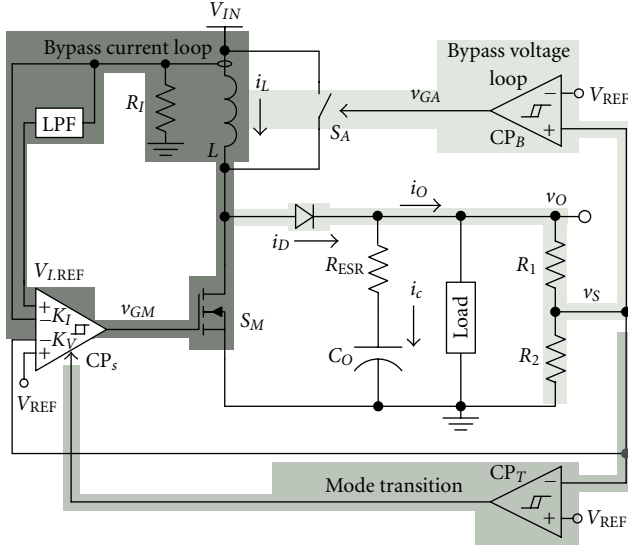


FIGURE 4: Simplified schematic of the proposed dual-mode $\Sigma\Delta$ boost converter.

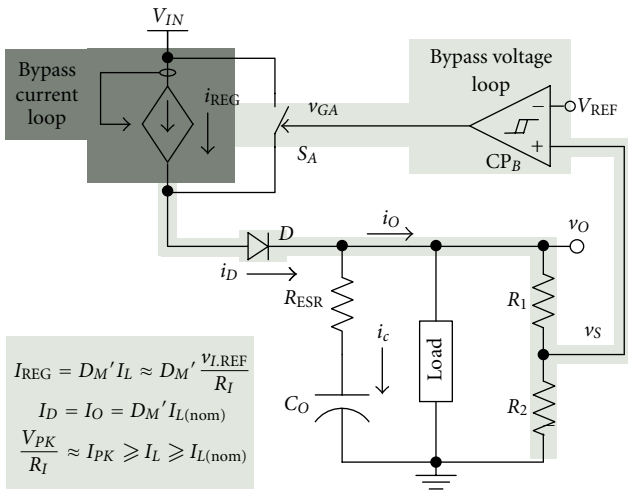


FIGURE 5: Equivalent circuit of the proposed $\Sigma\Delta$ converter in the bypass mode.

With respect to stability, as already mentioned, the unity-gain frequency of the current loop ($f_{i,0dB}$) must exceed that of the bypass voltage loop ($f_{b,0dB}$) so the inductor appears as a current source in the voltage loop, eliminating the complex conjugate pair associated with LC in the voltage loop [12]. Because the unity-gain bandwidth of a $\Sigma\Delta$ loop is its switching frequency, S_M 's switching frequency ($f_{i,0dB}$) must exceed that of S_A ($f_{b,0dB}$). Therefore, since $f_{i,0dB}$ depends on the rising and falling rates of $i_L R_I$ as it traverses CP_S 's hysteretic current window H_I ,

$$f_{i,0dB} = \left(\frac{H_I}{R_I}\right)^{-1} \left(\frac{L}{V_{IN}} + \frac{L}{V_O - V_{IN}}\right)^{-1} = \frac{V_{IN}(V_O - V_{IN})R_I}{V_O H_I L} \quad (6)$$

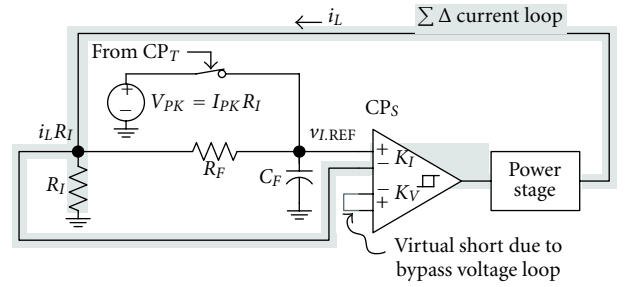


FIGURE 6: Simplified conceptual circuit schematic of the dual-mode $\Sigma\Delta$ converter in bypass mode, as the bypass loop virtually shorts v_s and V_{REF} and the current loop regulates i_L to $v_{I,REF}/R_I$.

and $f_{b,0dB}$ on how fast excess i_D (i.e., $D_M' I_L - I_D$) and I_O charge and discharge output capacitor C_O between CP_B 's hysteretic voltage window H_V ,

$$f_{b,0dB} = \left(\frac{H_V(R_1 + R_2)}{R_2}\right)^{-1} \left(\frac{C_O}{I_O} + \frac{C_O}{(D_M' I_L - I_O)}\right)^{-1}, \quad (7)$$

to force $f_{i,0dB}$ to be greater than $f_{b,0dB}$, C_O must exceed

$$C_O \geq \left(\frac{H_I}{H_V}\right) \left(\frac{I_O L}{V_O R_I D_M'}\right) \left(\frac{R_2}{R_1 + R_2}\right) \equiv C_{O(min)}, \quad (8)$$

where the R_1 - R_2 divider represents the effect of the resistive feedback factor on H_V and $C_{O(min)}$ the minimum stable output capacitance.

3.2. Transient Response and Mode Transition. During a positive load-dump event, when I_O suddenly rises and v_O droops in response, as shown in Figure 7, the dual-mode converter enters its bypass mode, raising i_L to peak value I_{PK} (or V_{PK}/R_I) in a single switching cycle of S_M . Subsequently v_O (or v_s) is pulled back to $V_{REF} (R_1 + R_2)/R_2$ (or V_{REF}) in a single switching cycle of S_A . Transient-detect comparator CP_T in Figure 4 perceives the load dump and engages the bypass mode by sensing when v_s drops below V_{REF} by a preset threshold value of ΔV_{BP} (e.g., 2.5% of V_{REF}) (after the delay the comparator requires to switch: t_d). Then, CP_T clamps $v_{I,REF}$ to peak voltage V_{PK} , the value of which sets the maximum current the circuit can drive. Switch S_M therefore remains closed ($t_{L(on)}$) until i_L reaches V_{PK}/R_I (I_{PK}), the new value of $v_{I,REF}/R_I$. After S_M resumes switching and regulating i_L about I_{PK} , S_A remains open and allows all diode current i_D to flow to v_O until C_O recharges to $(V_{REF} + H_V/2) \cdot (R_1 + R_2)/R_2$. Beyond this point, CP_B and S_A regulate v_s about V_{REF} by switching S_A , in other words, by steering excess inductor current away from C_O .

Ultimately, output voltage v_O droops in response to load dump Δi_O until i_L reaches I_{PK} . First, excess current Δi_O discharges C_O during delay t_d while v_s reaches $V_{REF} - \Delta V_{BP}$. Then, while S_M raises i_L from $i_{L(avg)}$ (or V_{REF}/R_I or $I_{L(nom)1}$) to

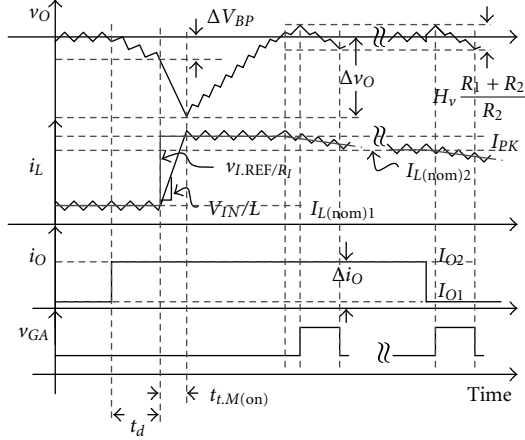


FIGURE 7: Transient-response performance when presented with fast load-steps (positive and negative).

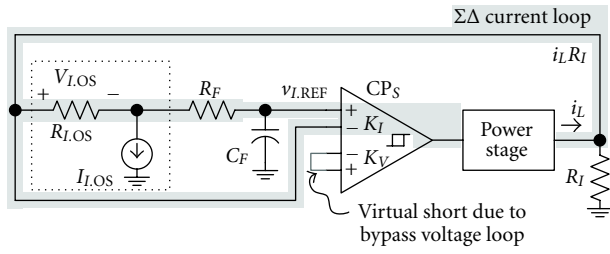


FIGURE 8: Equivalent converter circuit in bypass mode with added offset voltage $V_{L,OS}$ to ensure that $v_{L,REF}/R_I$ is slightly below $i_{L(av)}$.

I_{PK} (or V_{PK}/R_I), i_D is zero and full load current I_O discharges C_O , yielding a total variation (Δv_O) of

$$\begin{aligned} \Delta v_O &= \Delta V_{BP} + \left(\frac{I_O}{C_O} \right) t_{t,M(on)} \\ &= \Delta V_{BP} + \left(\frac{I_O}{C_O} \right) \left[\frac{(I_{PK} - I_{L(nom)})L}{V_{IN}} \right] \\ &= \Delta V_{BP} + \left(\frac{I_O}{C_O} \right) \frac{(V_{PK} - v_{L,REF})L}{R_I V_{IN}}. \end{aligned} \quad (9)$$

Note that the ratio of L and C_O sets the dominant part of Δv_O .

Once sensed output voltage v_S is within the hysteretic voltage window of CP_B , to transition back to steady state, $i_{L(av)}$ must somehow fall back to whatever value ($I_{L(nom)}$) is necessary to sustain I_O , reducing to zero the amount of excess current i_L that bypass comparator CP_B steers away from v_O through S_A . To that end, introducing a series negative offset voltage $V_{L,OS}$, as shown in Figure 8, ensures that i_L is always above its target (i.e., $i_{L(av)}$ is greater than $v_{L,REF}/R_I$), forcing the loop to gradually decrease both $i_{L(av)}$ and the excess current. Finally, when i_L is low enough to be able to fully supply i_O , and the excess current ($D'_M I_L - I_O$) is zero, the bypass loop stops switching (i.e., disengages), which means that the main voltage loop now regulates v_O via S_M (Figure 4) to its target. In other words, henceforth, $i_{L(av)}$ equals $I_{L(nom)}$.

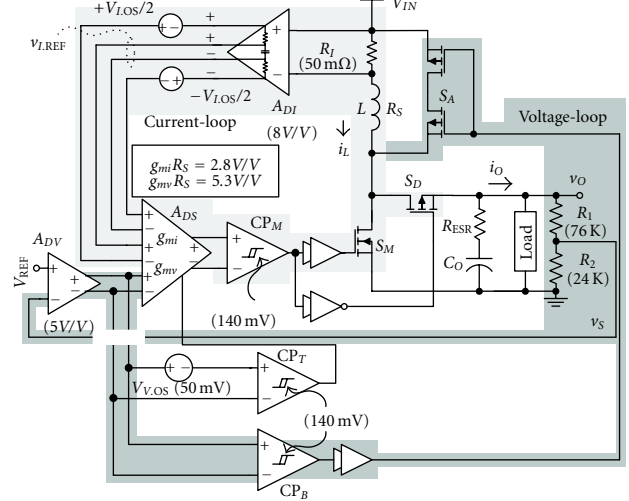


FIGURE 9: 0.5 μm CMOS circuit embodiment of the proposed dual-mode $\Sigma\Delta$ bypass boost converter.

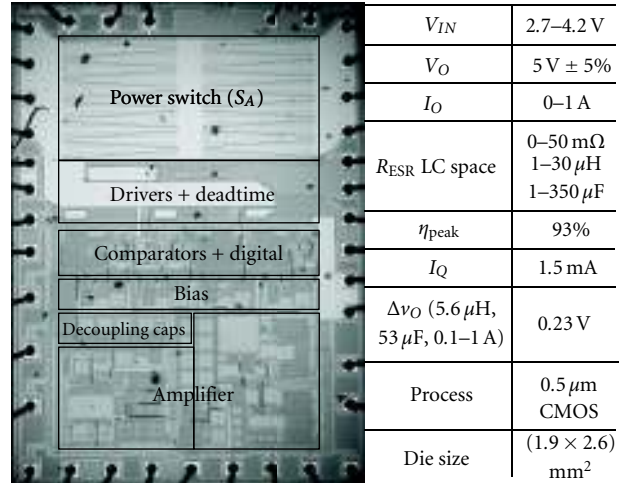


FIGURE 10: Die photograph and performance summary.

Note that the transition is continuous, allowing S_A to stop switching without incurring irregularities in S_M .

During a negative load dump, when i_O suddenly drops, as also shown in Figure 7, $i_{L(av)}$ automatically exceeds its new steady-state target and v_O rises above its target. As a result, bypass comparator CP_B engages and diverts current away from v_O until v_S again drops to $V_{REF} - H_V/2$ (in one cycle of S_A). The circuit gradually transitions back to steady state in the same manner as described earlier, through $V_{L,OS}$.

4. Experimental Results and Discussion

4.1. IC Design. The proposed dual-mode $\Sigma\Delta$ bypass converter was designed, fabricated, and evaluated using a 0.5 μm , 5 V CMOS process. The circuit embodiment of the converter, as shown in Figure 9, employs a differential-signal processing scheme to attenuate the effects of substrate noise on the high-bandwidth $\Sigma\Delta$ loops [10]. For simplicity, series resistor

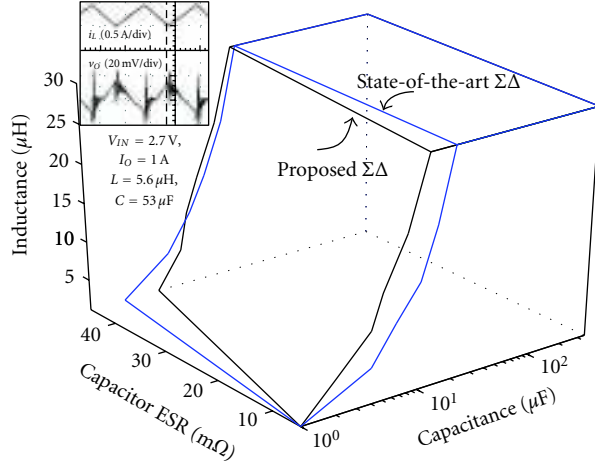


FIGURE 11: Nominal steady-state snapshot of inductor current i_L and output voltage v_O ripples (inset) for the proposed solution and experimental $R_{ESR}LC$ stability space for both the proposed dual- and state-of-the-art single-mode boost $\Sigma\Delta$ converters.

R_I senses i_L with the understanding more power efficient techniques are possible and recommended [13]. Current-sense amplifie A_{DI} , which monitors the voltage across R_I , includes an internal RC filter that generates differential current reference $v_{I,REF}$. Differential preamplifie A_{DV} buffers and amplifie sensed output voltage v_S by 5V/V to decrease the effects of offsets and hysteretic window limits in posterior amplifier and comparators on v_S and v_O (i.e., improve accuracy); A_{DV} drives differential summing amplifie A_{DS} , bypass hysteretic comparator CP_B , and transient-detect hysteretic comparator CP_B .

For ease of design and reliability, main, bypass, and transient-detect comparators CP_M , CP_B , and CP_T adopt the same circuit architecture, which is designed to yield a hysteretic window of 140 mV. The bypass threshold voltage (ΔV_{BP}) is composed of half the comparator hysteretic window plus an additional offset of 50 mV ($V_{V,OS}$) that is added between CP_B and CP_T . Differential current-sense amplifie A_{DI} includes a 40 mV offset voltage ($V_{I,OS}$) at its output to ensure i_L is below its target by $V_{I,OS}/R_I$ during the bypass mode, to gradually transition back to steady state after a load dump. The designed offsets are sufficiently large to dwarf the transistor mismatch-induced offsets in A_{DI} , CP_B , and CP_T and ensure that the polarities of $V_{V,OS}$ and $V_{I,OS}$ remain unchanged across process and temperature corners.

In the absence of deep-N or buried layer isolation structures, the bulk of a single PMOS transistor serving the function of auxiliary switch S_A could not be connected to the highest potential (v_O) because of latch-up concerns. Whenever the switching node flie above v_O following the turn-off of S_M , S_A 's body diode can conduct engaging the parasitic vertical PNP transistor present, channeling considerable current to the substrate. A second PMOS device is therefore added in series to use its reverse-biased body diode to block the foregoing current. And during normal

operating conditions, when v_O is higher than V_{IN} , as the body diode of the first blocks the current of the second.

The proposed $\Sigma\Delta$ controller 0.5 μm IC was designed to supply power from a 2.7–4.2 V Li-Ion battery and drive a 0–1 A load at $5V \pm 5\%$ with as wide an $R_{ESR}LC$ range as possible (0–50 m Ω , 1–30 μH , and 1–350 μF was achieved). The total silicon surface area the IC occupied was 1.9×2.6 mm (Figure 10). The peak efficiency of the converter was 93% at 0.4A with a biasing quiescent current of 1.5 mA. The total output voltage variation of the converter in response to a 0.1–1A load dump (Δi_O) with 5 m Ω , 5.6 μH , and 53 μF of $R_{ESR}LC$ was 200 mV, which constitutes a 4x improvement over its nonbypassed counterpart under similar conditions (800 mV).

4.2. LC Compliance. The measured $R_{ESR}LC$ space for which the converter was stable is 0–50 m Ω , 1–30 μH , and 1–350 μF , as illustrated in Figure 11. This range was determined by subjecting the converter to 0.1–1A load dumps with 100 nanoseconds rise and fall times. The stability limit was observed as a loss of regulation for the proposed $\Sigma\Delta$ converter in the bypass mode, as the bypass loop was no longer able to control the loop, and subharmonic oscillations for the nonbypassed (state-of-the-art) $\Sigma\Delta$ boost converter [14].

The stability limits for both converters, with and without the bypass path, are reached when their respective current-loop bandwidths ($f_{L,dB}$) approach their voltage-loop counterparts ($f_{B,dB}$ and $f_{V,dB}$), as that is when L ceases to be a current source for the voltage loop, be the main loop, or the bypass loop. As a result, because $f_{V,dB}$ and $f_{B,dB}$ increase with decreasing C_O and increasing I_O and $f_{L,dB}$ and RHP zero z_{RHP} decrease with increasing L and decreasing V_{IN} , the highest L - I_O (30 μH –1A) and lowest C_O - V_{IN} (12 μF –2.7V) combination constitutes worst-case conditions. Since R_{ESR} essentially introduces a left-half plane zero in the voltage loop, increasing R_{ESR} also increases $f_{V,dB}$ and $f_{B,dB}$, which means that the above-mentioned limits along with the highest R_{ESR} value (50 m Ω) describe the worst-case stability point of the converter. In other words, $C_{O(min)}$ increases with increasing L , I_O , and R_{ESR} and decreasing V_{IN} .

The maximum capacitance was limited to 350 μF as a practical limit for the intended portable application space (the circuit is stable at higher C_O values). Similarly, the maximum R_{ESR} value was limited to 50 m Ω to keep the output voltage ripple acceptably low under a 1A load. Under these conditions and constraints, the stability spaces for the proposed and the state-of-the-art converters are approximately equal in “volume.”

4.3. Transient Load-Dump Performance. As shown in Figure 12(a), the transient-response variation of v_O (Δv_O) in response to 0.1–1A load dumps (Δi_O) with 100 nanoseconds rise and fall times under 2.7V, 5.6 μH , 53 μF , and 5 m Ω of V_{IN} , L , C_O , and R_{ESR} was 200 mV for the proposed dual-mode scheme and 800 mV for its single-mode state-of-the-art counterpart. While the proposed converter responds by increasing i_L above its target (to I_{PK} or V_{PK}/R_I)

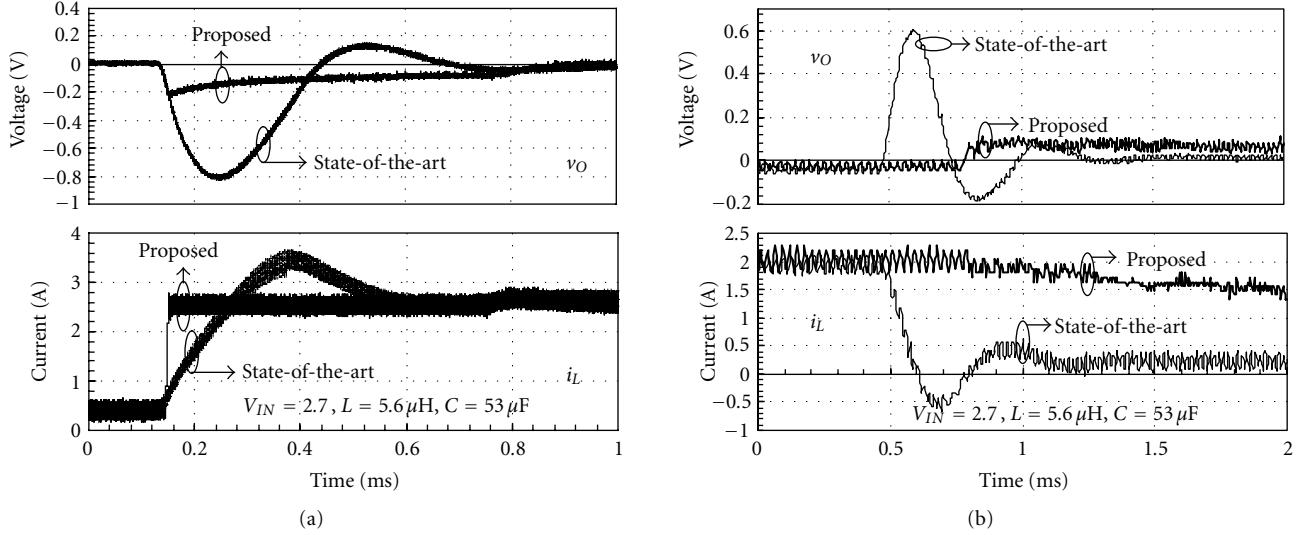


FIGURE 12: Measured transient performance of the proposed dual-mode and state-of-the-art single-mode $\Sigma\Delta$ boost converters in response to (a) 0.1–1 A and (b) 1–0.1 A load steps.

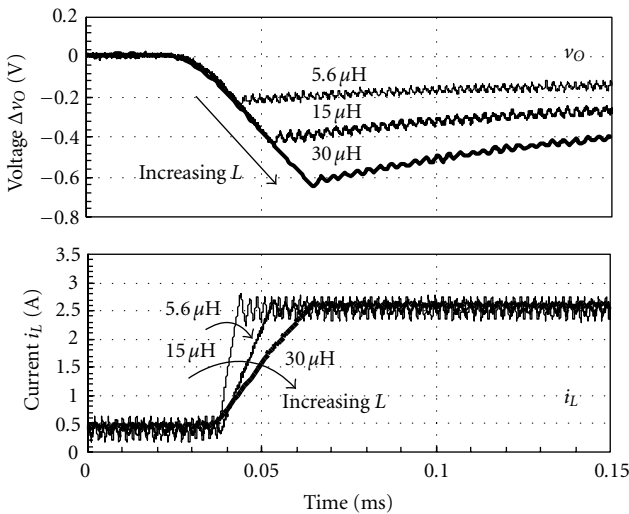


FIGURE 13: Measured effects of L on the transient performance of the proposed dual-mode $\Sigma\Delta$ bypass boost in response to 0.1–1 A load dumps, $C_O = 53 \mu\text{F}$.

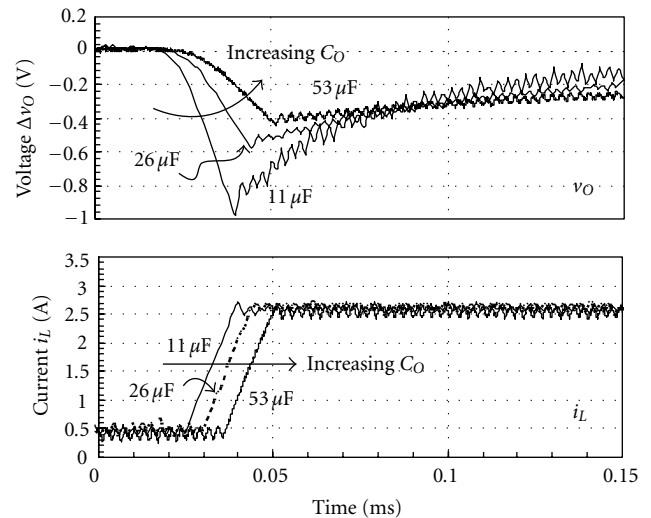


FIGURE 14: Measured effects of C_O on the transient performance of the proposed dual-mode $\Sigma\Delta$ bypass boost converter in response to 0.1–1 A load dumps.

in one switching cycle of S_M , the state-of-the-art circuit increases i_L gradually, pulling v_O back to regulation in several cycles of S_M , which is why the proposed solution exhibits a fourfold improvement over its predecessor. In a negative load-step (Figure 12(b)), while the excess inductor current is immediately bypassed by switch S_A in the proposed converter keeping the output voltage overshoot low ($<75 \text{ mV}$), the excess inductor energy causes a large voltage overshoot (600 mV) in the state-of-the-art converter.

Decreasing (increasing) L increases (decreases) the rate at which i_L responds to a load dump, as shown in Figure 13, thereby decreasing (increasing) the time v_O slews (reducing Δv_O). Similarly, increasing (decreasing) C_O decreases (increases) v_O 's droop rate in response to

a load dump (Figure 14). Note that increasing (decreasing) C_O also increases (decreases) the delay time between the load step and the onset of bypass threshold voltage $\Delta V_{BP}(t_d)$ (Figure 7), which is why the onset of i_L rising shifts with C_O .

Although transient-response performance for the proposed dual-mode scheme improves with decreasing L , the same is not true for the single-mode converter whose i_L response time is limited by the bandwidth of the loop, not L 's slew rate. As a result, as illustrated in Figure 15, the percentage improvement that the dual-mode enjoys over its single-mode counterpart increases with decreasing L : 6- and 1.43-fold improvement at $1 \mu\text{H}$ – $36 \mu\text{F}$ and $30 \mu\text{H}$ – $36 \mu\text{F}$, respectively.

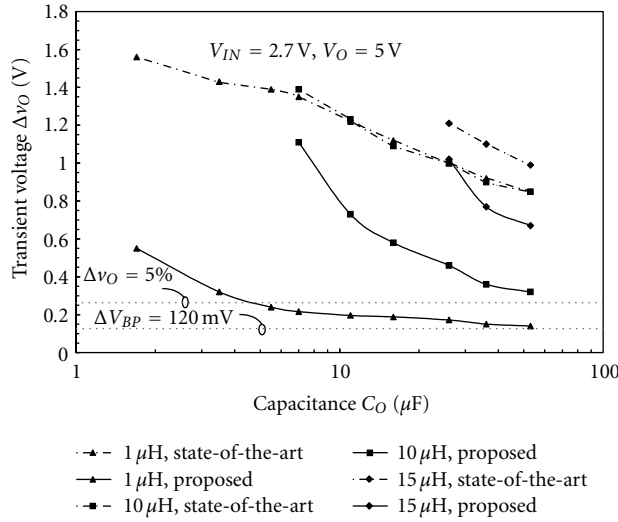


FIGURE 15: Measured transient output voltage variation Δv_O under various LC combinations in response to 0.1–1 A load dumps (Δi_O) for the proposed dual-mode and state-of-the-art single-mode $\Sigma\Delta$ converters.

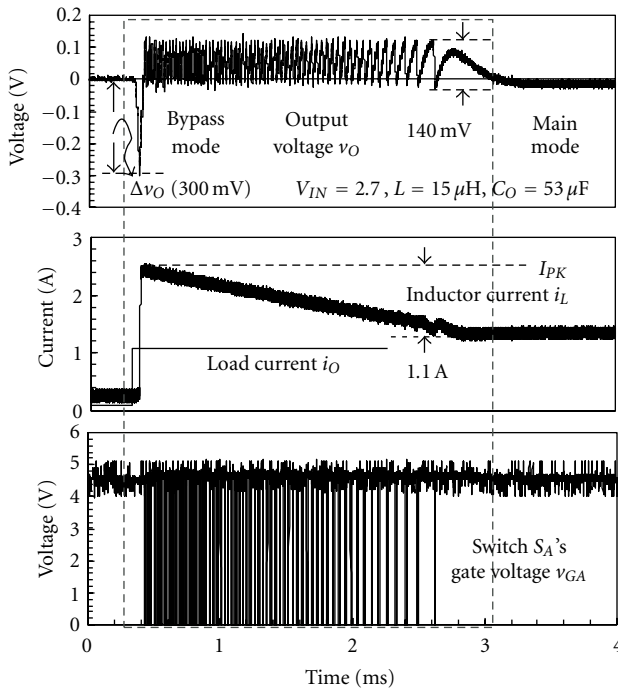


FIGURE 16: Measured steady state to bypass and back transitions in response to positive 0.1–0.6 A load dumps (positive Δi_O).

Increasing C_O decreases v_O 's transient droop in both converter cases, except that bypass threshold voltage ΔV_{BP} effectively limits the extent to which a larger C_O decreases Δv_O in the proposed scheme. In the limit, increasing C_O to such an extent that Δv_O is less than ΔV_{BP} would prevent the bypass mode from ever engaging. As a result, the performance improvement in Δv_O is lower between the

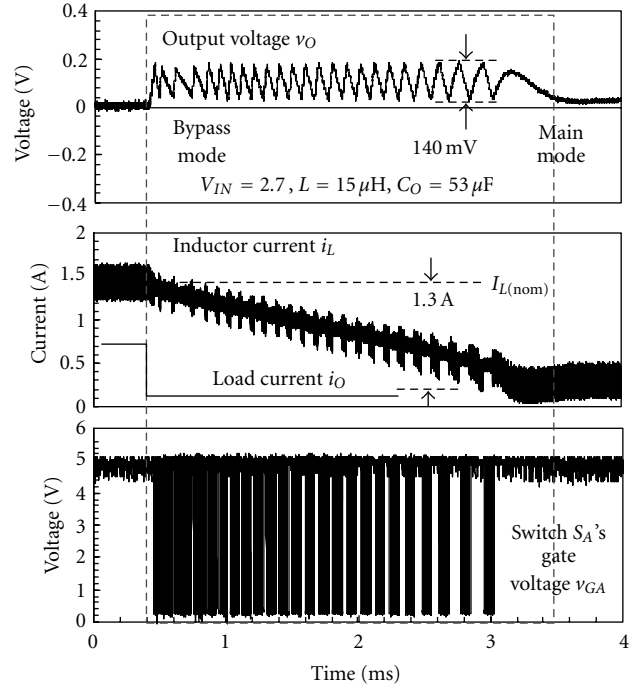


FIGURE 17: Measured steady state to bypass and back transitions in response to negative 0.6–0.1 A load dumps (negative Δi_O).

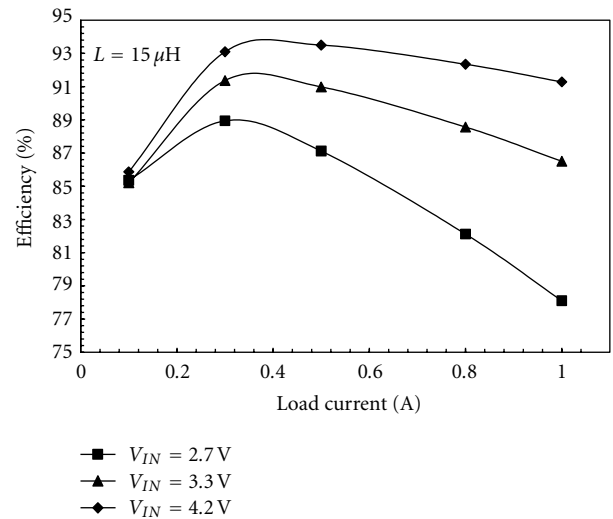


FIGURE 18: Measured steady-state efficiency Vs. Load current I_O for the proposed converter.

proposed and state-of-the-art solutions at higher C_O values: Δv_O for the proposed and state of the art asymptotically converge as C_O increases.

4.4. Mode Transition. Figures 16 and 17 illustrate how the proposed dual-mode $\Sigma\Delta$ bypass boost converter transitions from steady state to bypass mode and back in response to positive and negative 0.1–0.6 A load dumps with an LC combination of 15 μH and 53 μF . As designed, the bypass mode

ripple is larger at ± 70 mV ($\pm(H_V/2) \cdot (R_1 + R_2)/(R_2 A_{DV}) \approx \pm 140$ mV/2) or $\pm 1.4\%$ than the steady-state counterpart, which is at ± 15 mV or $\pm 0.3\%$. During a positive load dump (Figure 16), when i_O suddenly rises, a load-induced drop in v_O exceeding the ΔV_{BP} limit engages the bypass mode and increases i_L to 2.5 A (I_{PK}) in one switching cycle of S_M . As determined by offset V_{LOS} , the circuit then takes approximately 2.5 ms to gradually decrease i_L back to its new target of roughly 1.3A, at which point S_A stops switching and the converter is back in steady state. During a negative load dump (Figure 17), i_L is automatically above its target and S_A consequently starts diverting some of i_L back to V_{IN} almost immediately, until 2.5 ms later, when i_L drops to its new target.

The main drawbacks of the auxiliary bypass path are the silicon real estate, power, and switching noise associated with power switch S_A . The latter two shortcomings, however, are more often than not inconsequential because they only occur during transient events, which are typically sporadic, short, and seldom occur without significantly affecting the steady-state power efficiency (Figure 18). The prominent disadvantage of the proposed solution is therefore additional silicon real estate for S_A because it carries substantial current. The transient-performance benefit of S_A and the bypass path that drives it, however, offset this cost.

5. Conclusion

A dual-mode $\Sigma\Delta$ bypass boost dc-dc controller 0.5 μm CMOS IC that is stable for an $R_{ESR}LC$ filter range of 0–50 m Ω , 1–30 μH , and 1–350 μF and responds to positive and negative load dumps in one switching cycle has been proposed, designed, fabricated, and evaluated. The driving feature of the foregoing solution is a robust on-chip (i.e., smooth transitioning) $\Sigma\Delta$ bypass path that responds only during transient load dumps. While the converter increases inductor current i_L in one switching cycle in response to a sudden rise in load current i_O and uses it to quickly slew output capacitor C_O back to its target, it also limits how much of i_L flows to C_O in the case of a negative load dump, when i_O drops, limiting the total transient variation of output voltage v_O and therefore improving accuracy performance. The transient-response benefit of the proposed scheme, as compared to state-of-the-art single-mode $\Sigma\Delta$ converters, are the highest at low values of L (e.g., 6x at 1 μH and 1.41x or 40% improvement at 30 μH) because L limits how fast i_L rises and falls to its targets. The main drawback of the proposed technique is the additional silicon real estate required for auxiliary power switch S_A , which is partially (and often completely) offset by its improved accuracy performance. In summary, the proposed dual-mode $\Sigma\Delta$ bypass boost converter is fast, widely LC compliant (robust), and easily implementable.

Acknowledgment

This work was supported by Texas Instruments.

References

- [1] B. Schaffer, "Internal compensation—boon or bane?" in *Unitrode Design Seminar SEM 1400*, Texas Instruments, Dallas, Tex, USA, 2001.
- [2] M. Chen, J. P. Vogt, and G. A. Rincón-Mora, "Design methodology of a hybrid micro-scale fuel cell-thin-film Lithium Ion source," in *Proceedings of the 50th Midwest Symposium on Circuits and Systems (MWSCAS '07)*, pp. 674–677, Montreal, Canada, August 2007.
- [3] H.-P. Le, C.-S. Chae, K.-C. Lee, et al., "A single-inductor switching DC-DC converter with 5 outputs and ordered power-distributive control," in *Proceedings of the 54th IEEE International Solid-State Circuits Conference (ISSCC '07)*, pp. 534–620, San Francisco, Calif, USA, February 2007.
- [4] H. Sira-Ramírez, "Sliding mode- Δ modulation control of a "buck" converter," in *Proceedings of the 42nd IEEE Conference on Decision and Control*, vol. 3, pp. 2999–3004, Maui, Hawaii, USA, December 2003.
- [5] R. Miftakhutdinov, "Analysis of synchronous buck converter with hysteretic controller at high slew-rate load current transients," in *Proceedings of High Frequency Power Conversion Conference*, pp. 55–69, 1999.
- [6] B. Schweitzer and A. Rosenstein, "Free running—switching mode regulator: analysis and design," *IEEE Transactions on Aerospace*, vol. 2, pp. 1171–1180, 1964.
- [7] G. A. Rincón-Mora, "Self-oscillating DC-DC converters: from the ground up," in *Proceedings of IEEE Power Electronics Specialists Conference Tutorial (PESC '01)*, 2001.
- [8] S.-C. Tan, Y. M. Lai, M. K. H. Cheung, and C. K. Tse, "On the practical design of a sliding mode voltage controlled buck converter," *IEEE Transactions on Power Electronics*, vol. 20, no. 2, pp. 425–437, 2005.
- [9] R. Venkataramanan, A. Sabanovic, and S. Cuk, "sliding mode control of DC-to-DC converters," in *Proceedings of the International Conference on Industrial Electronics, Control and Instrumentation (IECON '85)*, vol. 1, pp. 251–258, San Francisco, Calif, USA, 1985.
- [10] N. A. Keskar and G. A. Rincón-Mora, "A compact 1–30 μH , 1–350 μF , 5–50 m Ω ESR compliant, 1.5% accurate 0.6 μm CMOS differential $\Sigma\Delta$ boost DC-DC converter," *Analog Integrated Circuits and Signal Processing*, vol. 54, no. 3, pp. 157–169, 2008.
- [11] R. Erickson, *Fundamentals of Power Electronics*, Chapman & Hall, New York, NY, USA, 1st edition, 1997.
- [12] N. Keskar and G. A. Rincón-Mora, "Self-stabilizing, integrated, hysteretic boost DC-DC converter," in *Proceedings of the 30th Annual Conference of IEEE Industrial Electronics Society (IECON '04)*, vol. 1, pp. 586–591, Busan, Korea, November 2004.
- [13] H. P. Forghani-Zadeh and G. A. Rincón-Mora, "Current-sensing techniques for DC-DC converters," in *Proceedings of the 45th Midwest Symposium on Circuits and Systems*, vol. 2, pp. 577–580, Tulsa, Okla, USA, August 2002.
- [14] J. Calvente, F. Guinjoan, L. Martinez, and A. Poveda, "Subharmonics, bifurcations and chaos in a sliding-mode controlled boost switching regulator," in *Proceedings of IEEE International Symposium on Circuits and Systems (ISCAS '96)*, vol. 1, pp. 573–576, 1996.